Available online at www.sciencedirect.com
ScienceDirect
Trans. Nonferrous Met. Soc. China 32(2022) 824−837
Transactions of Nonferrous Metals Society of China
www.tnmsc.cn

Effect of Al addition on microstructure and mechanical properties of Mg−Gd−Zn alloys

Zhi-bing DING[1,2], Shuai ZHANG[1,2], Yu-hong ZHAO[3], Dong-rui CHEN[1,2], Li-hua ZOU[1,2], Zhi-gang CHEN[1,2], Wen-min GUO[1,2], Zai-jun SU[1,2], Hua HOU[3]

1. College of Mechanical and Energy Engineering, Shaoyang University, Shaoyang 422000, China;
2. Key Laboratory of Hunan Province for Efficient Power System and Intelligent Manufacturing, Shaoyang University, Shaoyang 422000, China;
3. College of Materials Science and Engineering, North University of China, Taiyuan 030051, China

Received 20 March 2021; accepted 28 October 2021

Abstract: The microstructure evolution and mechanical properties of Mg−15.3Gd−1Zn alloys with different Al contents (0, 0.4, 0.7 and 1.0 wt.%) were investigated. Microstructural analysis indicates that the addition of 0.4 wt.% Al facilitates the formation of 18R-LPSO phase ($Mg_{12}Gd(Al,Zn)$) in the Mg−Gd−Zn alloy. The contents of $Al_{11}Gd_3$ and Al_2Gd increase with the increase of Al content, while the content of $(Mg,Zn)_3Gd$ decreases. After homogenization treatment, $(Mg,Zn)_3Gd$, 18R-LPSO and some $Al_{11}Gd_3$ phases are transformed into the high-temperature stable 14H-LPSO phases. The particulate Al−Gd phases can stimulate the nucleation of dynamic recrystallization by the particle simulated nucleation (PSN) mechanism. The tensile strength of the as-rolled alloys is improved remarkably due to the grain refinement and the fiber-like reinforcement of LPSO phase. The precipitation of the β' phase in the peak-aged alloys can significantly improve the strength. The peak-aged alloy containing 0.4 wt.% Al achieves excellent mechanical properties and the UTS, YS and elongation are 458 MPa, 375 MPa and 6.2%, respectively.
Key words: Mg−Gd−Zn−Al alloy; long-period stacking ordered (LPSO) phase; β' phase; mechanical properties

1 Introduction

Currently, weight reduction is a major design consideration in the aerospace, automotive and 3C industries due to the strict requirements on the greenhouse gas emissions and fuel economy. Mg-based alloys are usually considered as promising structural materials due to their low densities, good damping capacity, and distinct strength [1−4]. Previous studies suggested that rare earth elements like Ce, Gd, Y and Nd can enhance the mechanical properties of magnesium alloys [5−8]. Mg−Gd−Zn alloys are considered particularly promising because of their satisfactory combination of high strength, ductility and creep resistance [9,10]. These excellent properties are attributed to the formation of the long-period stacking ordered (LPSO) phase and the β' phase. In the Mg−Al−Gd system, KISHIDA et al [11,12] identified a new LPSO phase with composition of Mg−6.8at.%Al−10.8at.%Gd, and described its structure as the 18R crystal structure based on order−disorder theory. Then, 14H LPSO with the ideal chemical formula of Mg−7.1at.%Al−9.5at.%Gd was found in the Mg−Al−Gd system [13]. Unfortunately, there are few further studies on the Mg−A1−Gd LPSO phase.

It has been found in recent studies that Al has a significant grain refinement effect on the Mg−RE

Corresponding author: Zhi-bing DING, Tel: +86-19848170538, E-mail: dzbing1992@163.com;
Yu-hong ZHAO, Tel: +86-351-3557006, E-mail: zhaoyuhong@nuc.edu.cn
DOI: 10.1016/S1003-6326(22)65836-9

alloys due to the formation of Al_2RE phase, which can be explained by edge-to-edge matching (E2EM) model [14,15]. QIU et al [16,17] identified the Al_2Y phase as an active nucleant through crystallographic calculation. Adding 0.6−1.0 wt.% Al to the Mg−10Y alloy can significantly reduce the grain size from 180 to 36 μm. The grain refinement efficiency of Al_2Gd and Al_2Y phases in Mg−RE alloys were equivalent to that of Zr, and the fine grains in Mg−RE−Al alloys were more thermally stable than those in Mg−RE−Zr alloys [18]. The results of ZHAO et al [19] showed that the addition of trace Y to the AZ91D alloy will form some rod-like Al_2Y phases, and the tensile properties have been significantly improved due to the grain refinement of Al_2Y phases. Moreover, it was suggested that the addition of trace Al to the Mg−5Gd−2.5Y−2Zn alloy can significantly improve the ductility and rollability, because $Al_2(Y,Gd)$ and $Al_{11}(Y,Gd)_3$ phases were formed and $(Mg,Zn)_3(Y,Gd)_2$ phases was suppressed [20].

Up to now, there have been few studies on the grain refinement of Mg−RE−Zn alloys by Al addition, and few details about the effect of Al addition on the formation of LPSO phase. In this work, the microstructure and mechanical properties of Mg−Gd−Zn−*x*Al (*x*=0, 0.4, 0.7 and 1.0, wt.%) alloys from the as-cast, as-homogenized, as-rolled and rolled−aged conditions were systematically investigated.

2 Experimental

The Mg−15.3Gd−1Zn−*x*Al (*x*=0, 0.4, 0.7 and 1, wt.%) alloys were fabricated using pure Mg, Zn, Al, and Mg−30wt.%Gd master alloys. These alloys, 90 mm in diameter and 150 mm in length, were prepared in an intermediate frequency induction furnace under Ar atmosphere and cooled in brine. The chemical compositions of the investigated alloys are listed in Table 1. The as-cast ingots were homogenized at 520 °C for 10 h, quenched into water, and then machined into plates with dimensions of 85 mm × 20 mm × 7.5 mm. The as-homogenized plates were preheated at 500 °C for 30 min before hot rolling. Then, the plates were rolled by equal speed rolling at 500 °C from 7.5 to 2.0 mm after about 15 passes, with a total plastic deformation of 73%. During each rolling pass, the rolled specimens were reheated at 500 °C for 10 min. The rolling specimens were cooled in air after the final rolling pass. Some of as-rolled sheets were aged at 220 °C with different ageing time.

Table 1 Chemical compositions of cast Mg−Gd−Zn(−Al) alloys (wt.%)

Alloy	Nominal composition	Chemical composition			
		Mg	Gd	Zn	Al
A	Mg−15.3Gd−1Zn	Bal.	15.40	1.04	−
B	Mg−15.3Gd−1Zn−0.4Al	Bal.	15.36	1.01	0.37
C	Mg−15.3Gd−1Zn−0.7Al	Bal.	15.28	1.05	0.75
D	Mg−15.3Gd−1Zn−1Al	Bal.	15.33	1.02	1.14

The microstructures of the specimens were characterized by optical microscopy (OM, DM2500M), scanning electron microscopy (SEM, SU5000 with a backscatter electron (BSE) detector), and energy dispersive spectroscopy (EDS). Secondary phases were identified by X-ray diffraction (XRD, Rigaku D/MAX2500PC) with a copper target. Macro-texture tests were conducted by using a PANalytical XPert MPD. Electron back scattered diffraction (EBSD) observation was conducted on a Hitachi S−3400N SEM equipped with a HKL-EBSD system. The detailed microstructures of the samples were further examined under transmission electron microscopy (TEM, JEM−2100F) at an accelerating voltage of 200 kV. The average grain size was calculated by analyzing the optical micrographs with the Image Pro Plus software. At least 300 grains were counted for each alloy. Vickers hardness testing was conducted under the load of 1.96 N and holding time of 15 s, in which each sample was measured at least 6 times. Tensile specimens were processed into the sheets of 15 mm in length, 4 mm in width and 2 mm in thickness with the long axis parallel to the rolling direction (RD). All tensile tests with an initial strain rate of 1.5 mm/min were carried out on a SHIMADZU AG-X plus testing machine. The ultimate tensile strength (UTS), yield strength (YS, offset of 0.2%) and elongation are the average values of repeated tests of at least three specimens.

3 Results and discussion

3.1 Microstructures of as-cast and as-homogenized alloys

Figure 1 shows the OM and SEM-BSE images

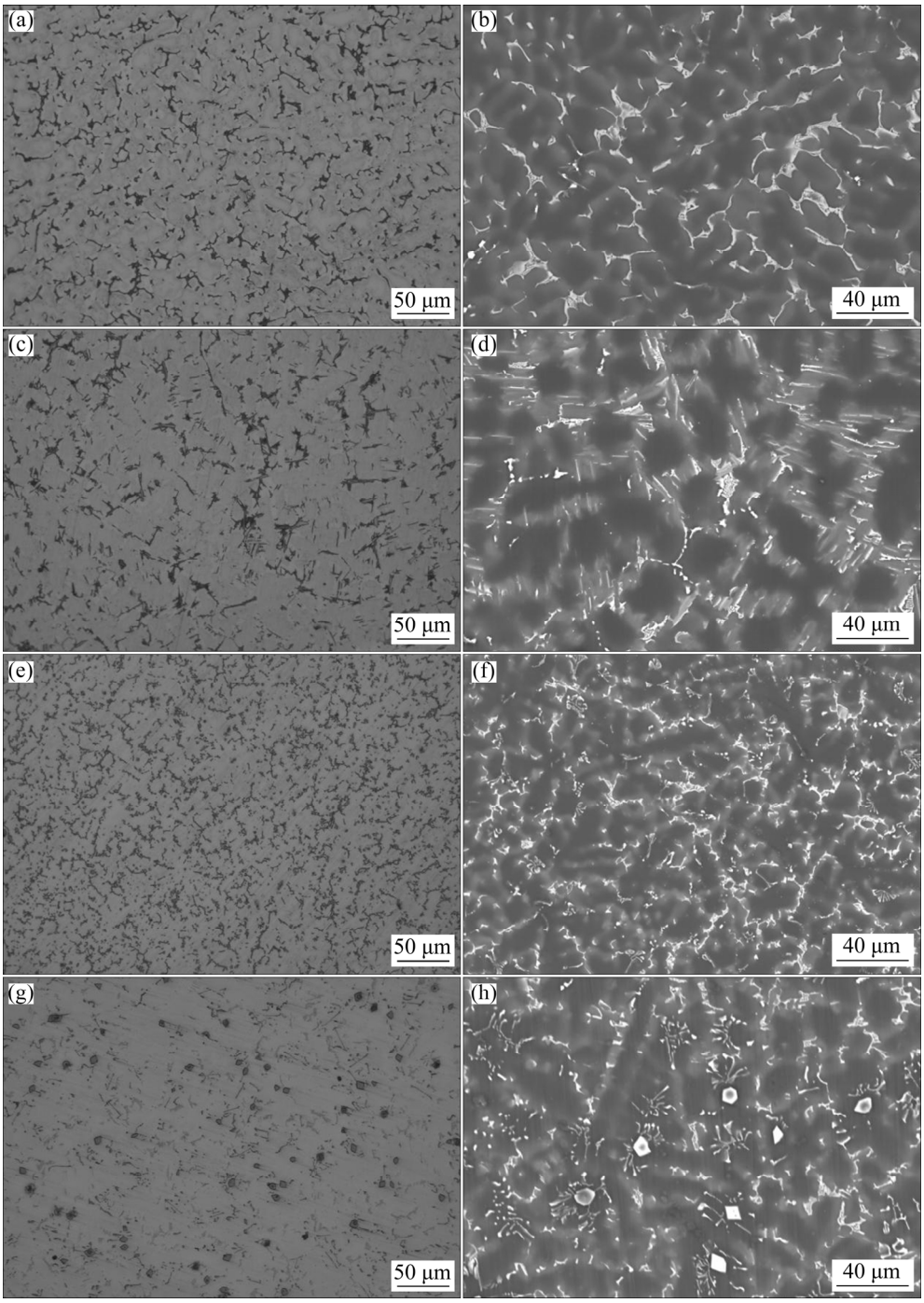

Fig. 1 Optical and SEM-BSE images of as-cast Mg−Gd−Zn(−Al) alloys: (a, b) Alloy A; (c, d) Alloy B; (e, f) Alloy C; (g, h) Alloy D

of the as-cast Mg−Gd−Zn(−Al) alloys. All the microstructures are composed of α-Mg dendrites and amounts of eutectics distribute along the grain boundaries discontinuously. In Alloy A, the eutectic phases distribute at the grain boundaries with a hollow-out skeleton morphology. In Alloy B, the majority of the eutectic phases are observed with bright and gray contrast distributing along the grain boundaries, and some clustered phases notably appear, as shown in Fig. 1(d). In the case of Alloys C and D with increased Al content, the amount of bright hollow-out skeleton phases decreases, the gray phases completely disappear, and the amount of clustered phases increases. Meanwhile, some polygonal phases are formed in the matrix, especially in Alloy D.

Figure 2 shows the magnified SEM-BSE micrographs of as-cast alloys, and the corresponding

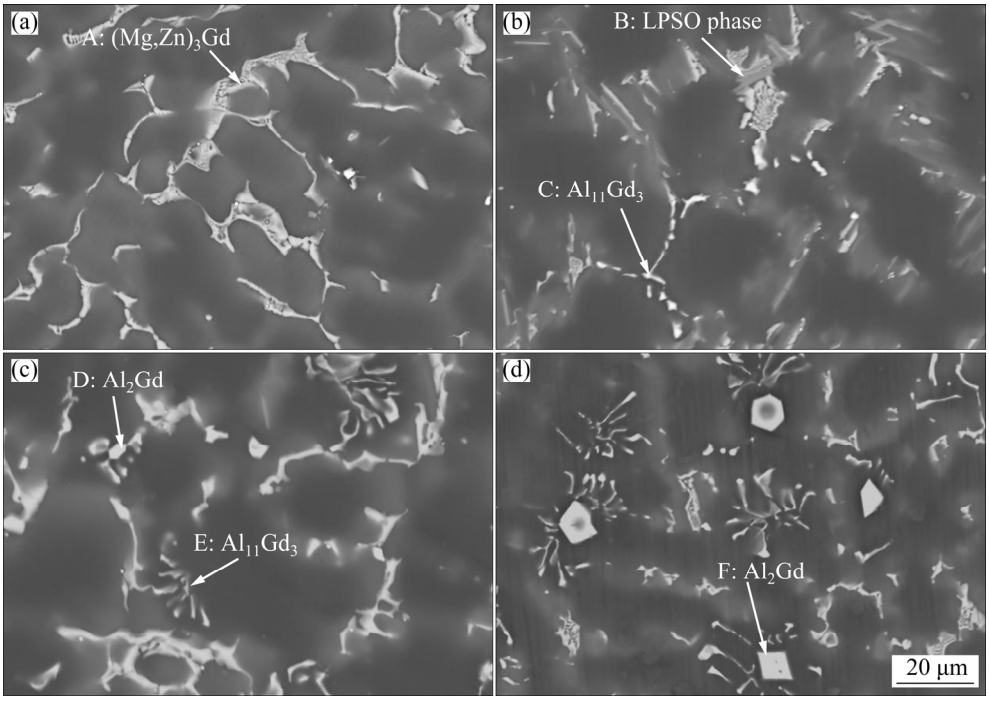

Fig. 2 Magnified SEM-BSE images of as-cast Mg−Gd−Zn(−Al) alloys: (a) Alloy A; (b) Alloy B; (c) Alloy C; (d) Alloy D

EDS results are summarized in Table 2. Combined with the XRD curves given in Fig. 3(a), the hollow-out skeleton phase, gray phase, clustered phase and polygonal phase are identified as *W* phase ($(Mg,Zn)_3Gd$), LPSO phase, $Al_{11}Gd_3$ and Al_2Gd, respectively. The LPSO phase usually presents the 18R-LPSO structure in as-cast alloys [21−23]. BIAN et al [22] and FANG et al [23] studied the microstructure of Mg−RE−Zn−Al alloys and reported that the 18R-LPSO phase did not contain Al element. However, the EDS analysis illustrates that the ratio of Al to Zn is approximately 1 and the ratio of (Al+Zn) to Gd also is approximately 1 for the LPSO phase in the Alloy B.

Table 2 EDS elemental analysis results of phase in as-cast alloys marked as A−F in Fig. 2

Point	Chemical composition/at.%				Possible phase
	Mg	Gd	Zn	Al	
A	82.53	11.89	5.58	−	$(Mg,Zn)_3Gd$
B	88.94	6.29	2.42	2.35	$Mg_{12}Gd(Al,Zn)$
C	69.12	8.60	1.60	20.68	$Al_{11}Gd_3$
D	50.62	14.34	1.08	33.96	Al_2Gd
E	76.96	5.86	0.96	16.22	$Al_{11}Gd_3$
F	56.22	13.99	1.43	28.36	Al_2Gd

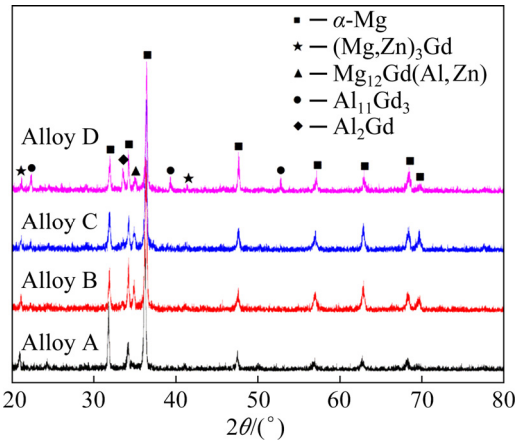

Fig. 3 XRD patterns of as-cast Mg−Gd−Zn(−Al) alloys

This suggests that the LPSO phase is $Mg_{12}Gd(Al,Zn)$. Interestingly, polygonal Al_2Gd phases mainly distribute in the matrix, and the $Al_{11}Gd_3$ phases cluster around the Al_2Gd phases, as shown in Figs. 2(c, d).

The addition of Al has a significant effect on the microstructures of the as-cast Mg−Gd−Zn alloys. In summary, with the increase of Al content, the order of transformation of the eutectic phase in the four as-cast alloys is $(Mg,Zn)_3Gd \rightarrow (Mg,Zn)_3Gd + Mg_{12}Gd(Al,Zn) + Al_{11}Gd_3 \rightarrow (Mg,Zn)_3Gd + Al_{11}Gd_3 + Al_2Gd \rightarrow (Mg,Zn)_3Gd + Al_{11}Gd_3 + Al_2Gd$. Some LPSO phases are found in

the microstructure of Alloy B, but not in the other three alloys. Due to the radius difference between Al (0.143 nm) and Mg (0.160 nm), adding trace Al can lead to lattice distortion and promote the formation of more stacking faults, which contribute to the formation of LPSO phase [24,25]. Similar phenomenon was reported by BIAN et al [22]. Obviously, the secondary dendrite arm spacing of Alloys C and D is finer than that of Alloys A and B, which may be attributed to the formation of Al_2Gd phase [20,26].

Figure 4 shows the SEM-BSE micrographs of the as-homogenized Mg−Gd−Zn(−Al) alloys. As can be observed in Figs. 4(a, b), many of the lamellar and bulk phases distribute discontinuously along the grain boundaries, and the parallel lamellar phases are inclined to be contacted and combined into bulk phases. Compared with Alloy A, the

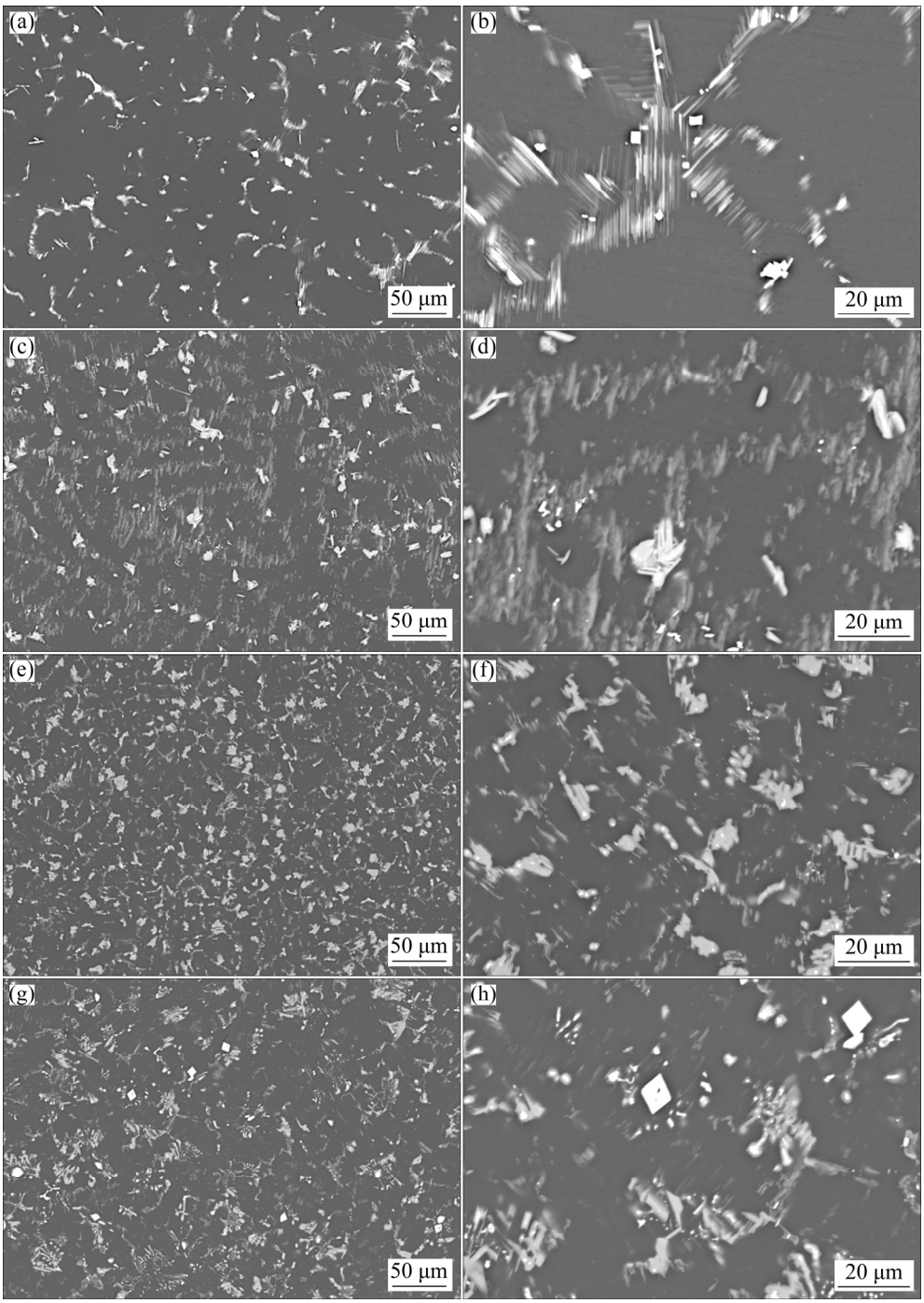

Fig. 4 SEM-BSE images of as-homogenized Mg−Gd−Zn(−Al) alloys: (a, b) Alloy A; (c, d) Alloy B; (e, f) Alloy C; (g, h) Alloy D

lamellar phases in Alloy B exhibit larger density and thickness, and the bulk phases are more pronounced. However, there are numerous bulk phases distributing along the grain boundaries in Alloy C, with only a small amount of lamellar phases. The bulk and lamellar phases in the as-homogenized Mg−Gd−Zn(−Al) alloys are correspondingly 14H-LPSO phases [27−29]. The bright-field TEM image in the as-homogenized Alloy B and the corresponding SAED pattern of the LPSO phase ($\boldsymbol{B}$//$[11\bar{2}0]_{\alpha}$) are shown in Fig. 5. The weak periodic diffraction spots of the 14H-LPSO phase locate at the positions of $n/14$ of $(0002)_{\alpha\text{-Mg}}$ fundamental diffraction. This result indicates that the hollow-out skeleton $(Mg,Zn)_3Gd$ and some clustered $Al_{11}Gd_3$ phases are transformed into the 14H-LPSO phases. The element map distribution of the as-cast and as-homogenized Alloy B is shown in Fig. 6. Most of Al elements in the as-cast alloy distribute in the clustered $Al_{11}Gd_3$ phase, and a few of them distribute in the *W* phase and the LPSO phase, as shown in Fig. 6(b). Zn and Gd elements mainly distribute in the *W* phase, and some of the Gd elements also obviously distribute in the clustered $Al_{11}Gd_3$ phase, as shown in Figs. 6(c, d). After homogenization treatment, the elements Al, Zn and Gd evenly distribute in the bulk and lamellar LPSO phases, as shown in Figs. 6(f−h). As for the as-homogenized Alloy D, the polygonal Al_2Gd and some clustered $Al_{11}Gd_3$ phases still present in the matrix, except for the bulk and lamellar LPSO phases, as shown in Figs. 4(g, h). In addition, some cuboid phases mainly distribute along the grain boundaries, which can be observed

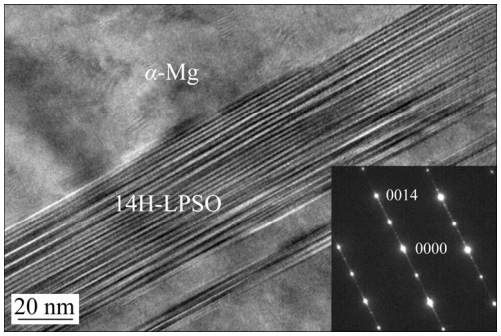

Fig. 5 Bright-field TEM image and corresponding SAED pattern of LPSO phase ($\boldsymbol{B}$//$[11\bar{2}0]_{\alpha}$) in as-homogenized Alloy B

in all as-homogenized alloys. It is a face-centered cubic (fcc) crystal structure with a=0.56 nm, and its composition is identified by EDS as a Gd-rich compound of Mg−87.38Gd−0.76Al−0.78Zn (wt.%) by EDS.

Previous studies have suggested that the formation of bulk and lamellar 14H-LPSO phases is mainly determined by the spinodal decomposition mechanism and the precipitation mechanism, respectively [28]. After homogenization treatment, the hollow-out skeleton $(Mg,Zn)_3Gd$ phases in as-cast Alloy A are mainly transformed into the lamellar 14H-LPSO phases. With the increase of Al content from 0 to 0.7 wt.%, the sum fraction of 14H-LPSO phase increases obviously, especially the bulk 14H-LPSO phase. These findings imply that Al can facilitate the formation of 14H-LPSO phase in the as-homogenized alloys, and the $Al_{11}Gd_3$ phase is mainly transformed into the bulk 14H-LPSO phase by a spinodal decomposition

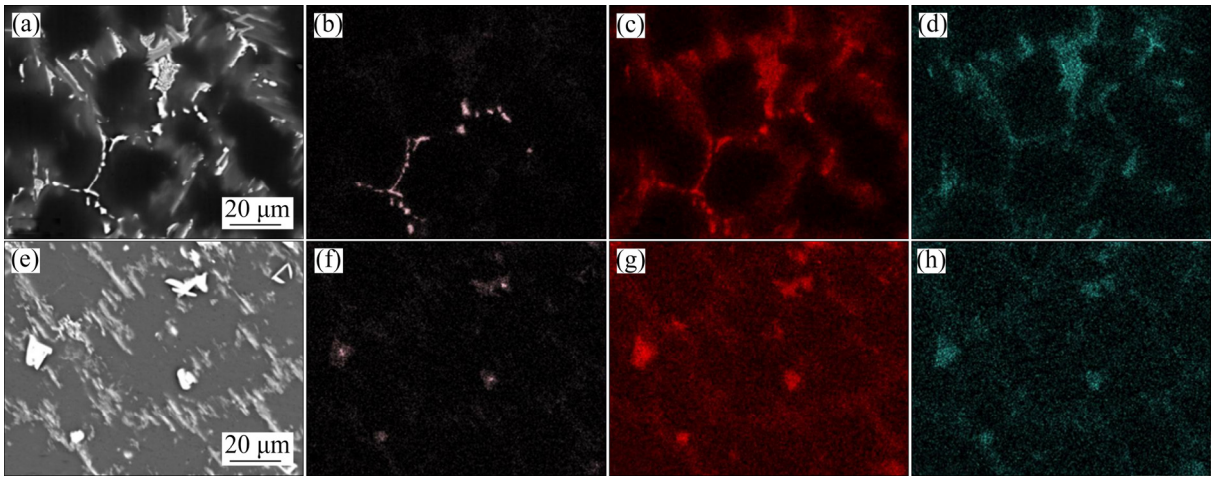

Fig. 6 SEM images (a, e) with element map distributions of as-cast (a−d) and as-homogenized (e−h) Alloy B: (b, f) Al; (c, g) Gd; (d, h) Zn

mechanism. There are some large-sized polygonal Al_2Gd phases in the as-homogenized alloy as they exist in the as-cast alloy, indicating that the Al_2Gd phase has good high-temperature stability, as shown in Figs. 2(d) and 4(h). Most of the $Al_{11}Gd_3$ phases are transformed into the LPSO phases after homogenization treatment, but some of them remain clustered in the matrix, especially in Alloy D. Therefore, the LPSO phase in Alloy D is less than that in Alloys B and C.

3.2 Microstructure and texture of as-rolled alloys

Figure 7 shows the optical images of the RD−ND plane of the as-rolled Mg−Gd−Zn(−Al) alloys. After the multi-pass hot rolling process at 500 °C, all the as-rolled alloys exhibit a finer and more uniform microstructure, indicating that the dynamic recrystallization (DRX) occurs during hot

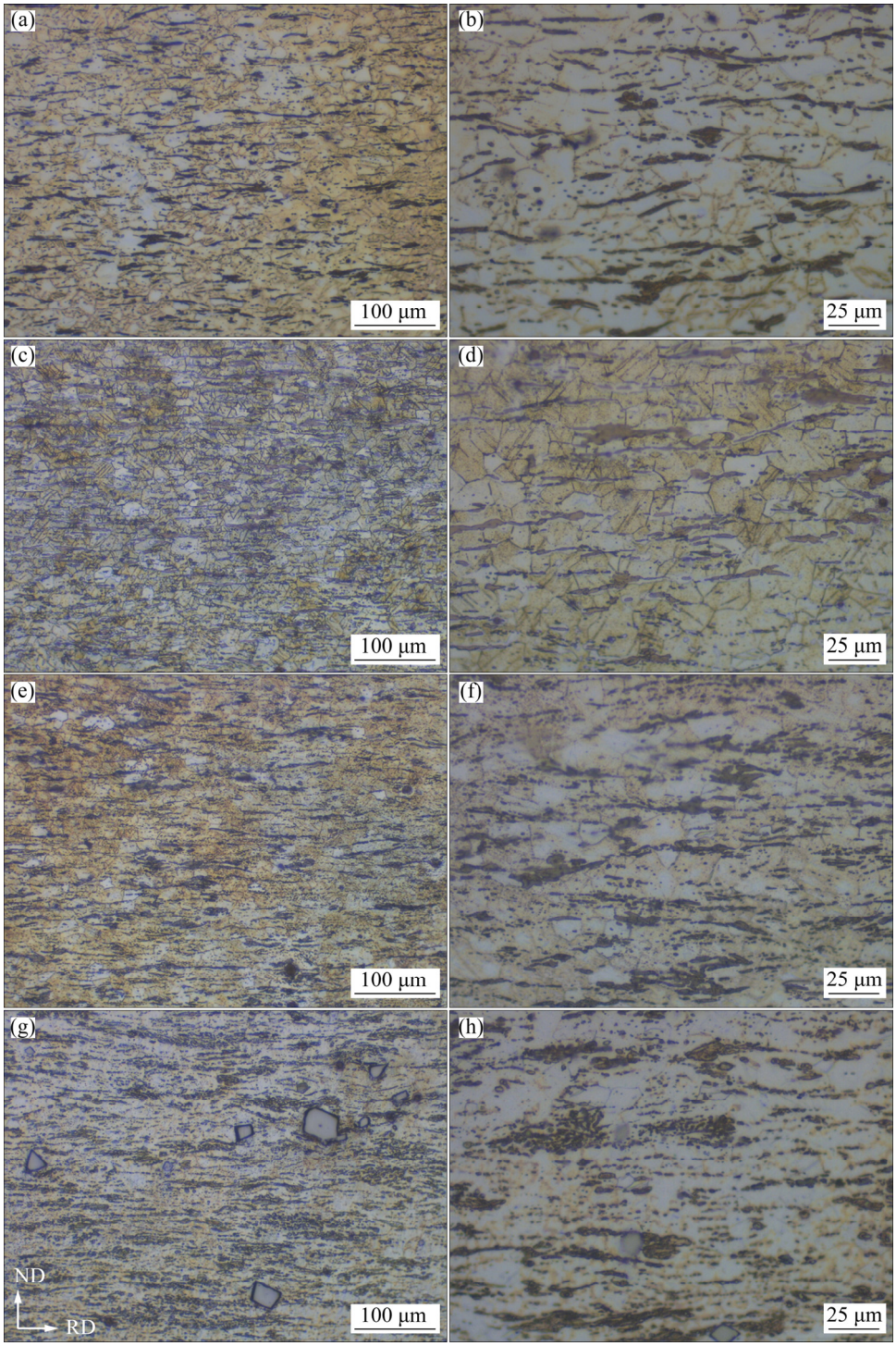

Fig. 7 Optical images of as-rolled Mg−Gd−Zn(−Al) alloys: (a, b) Alloy A; (c, d) Alloy B; (e, f) Alloy C; (g, h) Alloy D

rolling. Many interdigitated twins are observed in DRXed grains, especially in Alloy B. The average DRXed grain sizes of Alloys A, B, C and D are approximately 22.28, 18.40, 15.76 and 19.85 μm, respectively. In addition, a large number of continuous plate-shaped phases are parallel to the RD at the grain boundary, indicating that bulk LPSO, lamellar LPSO and clustered $Al_{11}Gd_3$ phases can be crushed by rolling force. It is noted that the thickness of the plate-shaped phase increases with the increase of Al content from 0 to 0.7 wt.%, due to the increase of the amount of LPSO phase. The thickest plate-shaped phase exists in Alloy D, which is the result of the coexistence of LPSO phase, $Al_{11}Gd_3$ phase and Al_2Gd phase. There is no difference in appearance of the Al_2Gd phase before and after hot rolling, as shown in Figs. 7(g, h).

Figure 8 shows the {0002} pole figures of the RD−TD plane of the as-rolled Mg−Gd−Zn(−Al) alloys. All the as-rolled alloys exhibit a typical basal texture with the (0002) basal plane of magnesium crystal parallel to the RD−TD plane (the (0002) basal plane of magnesium crystal perpendicular to the ND direction). There is obvious mountain-like images in the center of the circle (ND direction), which more vividly shows that the (0002) base plane of magnesium crystal is perpendicular to the ND direction, which is intuitively shown in the 2.5D pole figures. The basal poles spreading from ND toward TD are much wider than that toward RD, with an elliptical orientation distribution of the basal texture, which is a typical characteristic of RE-containing Mg alloys [30,31]. Interestingly, the position of maximum intensity of Alloy A almost has no inclination relative to the ND, exhibiting a single peak texture, as shown in Figs. 8(a, e). The position of maximum intensity of Al-containing alloys tilts about 2°−15° from the ND toward RD and TD, presenting a multi-peak morphology, as shown in Figs. 8(b−d, f−h). It is noteworthy that the maximum texture intensity decreases gradually with the Al addition, and the Alloy D has the smallest maximum texture intensity of 4.8. It is generally believed that the particle stimulated nucleation (PSN) plays an important role in promoting DRX and grain refinement [32,33]. FANG et al [23] reported that the addition of 1 wt.% Al elements to Mg−8Gd−5Y−2Zn alloy significantly weakened the maximum texture intensity from 15.1 to 3.9, because the particle $Al_{11}RE_3$ and Al_2RE phases within the grain have great effect on particle stimulated recrystallization. In the present study, the $Al_{11}RE_3$ and Al_2RE phases mainly distribute in Alloy D with the lowest maximum texture intensity.

Figure 9 shows the inverse pole figure (IPF) map, pole figures and relative Schmid factor distribution of the as-rolled Alloy B. As shown in

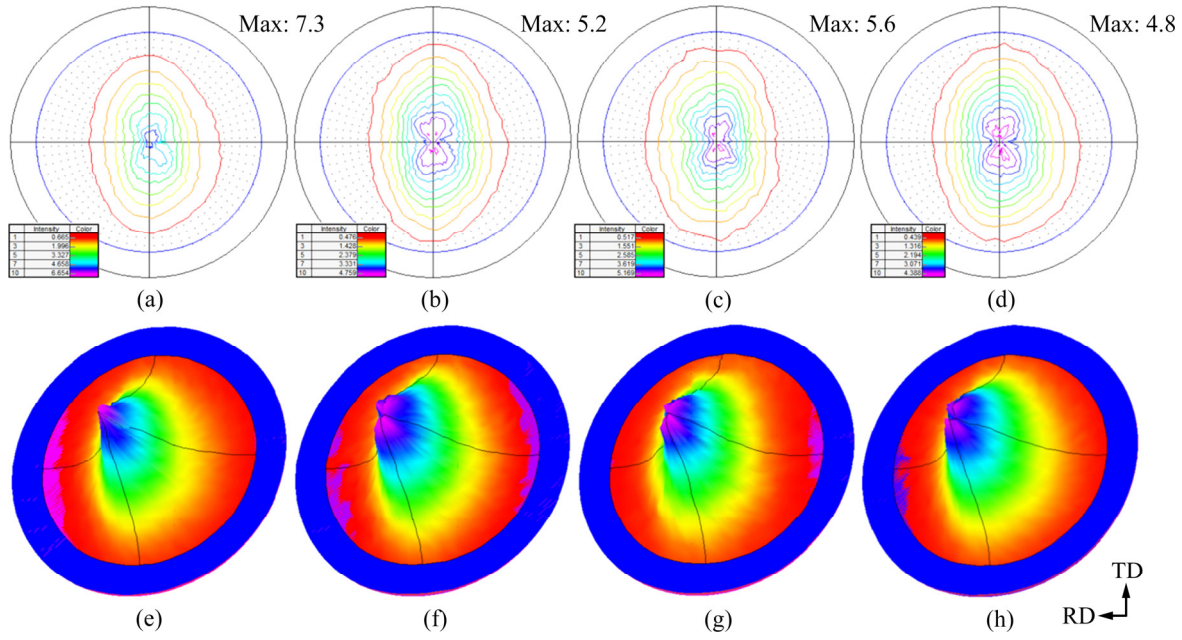

Fig. 8 2-dimensional (2D) (a−d) and 2.5-dimensional (2.5D) (e−h) pole figures of (0002) plane of Mg−Gd−Zn(−Al) alloys: (a, e) Alloy A; (b, f) Alloy B; (c, g) Alloy C; (d, h) Alloy D

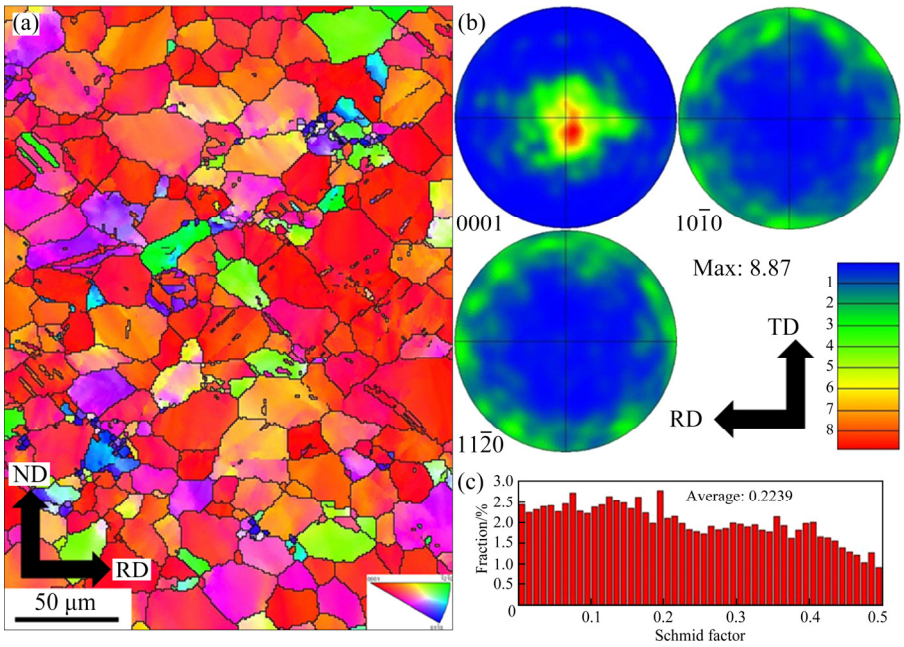

Fig. 9 EBSD analysis results of as-rolled Alloy B: (a) IPF image; (b) (0001), $(10\bar{1}0)$ and $(11\bar{2}0)$ pole figures; (c) $(0001)\langle 11\bar{2}0\rangle$ Schmid factor distributions

Figs. 9(a, b), the microstructure of the as-rolled alloy is composed of DRXed grains with a typical basal texture, which is consistent with Figs. 7 and 8. Some fine grains with a $(01\bar{1}0)$ prismatic plane parallel to the ND−RD plane are observed. These fine grains can effectively shorten the slip distance of dislocations, release the stress concentration at grain boundaries and improve the ductility of the alloy [34]. Many $\{10\bar{1}2\}$ extension twins are observed in the DRXed grains. Generally, the $\{10\bar{1}2\}$ extension twins with lower activation energy are often produced during compression deformation [31,34]. The Schmid factor is usually related to the texture and stress state of the alloy. Most of the grains have low Schmid factor values with a peak ranging from 0.00 to 0.17, as shown in Fig. 9(c). It is indicated that a weak texture is developed in the as-rolled alloy and the basal slip of grains is difficult to activate.

3.3 Aging hardening behaviors of as-rolled alloys and microstructures of peak-aged alloys

Figure 10 shows the age-hardening curves of the as-rolled Mg−Gd−Zn(−Al) alloys aged at 220 °C. Alloy A exhibits a significant age hardening response; the hardness increases rapidly within 0−20 h, and reaches a peak hardness of HV 137.10 after 23 h. The peak hardness of the as-rolled Alloy

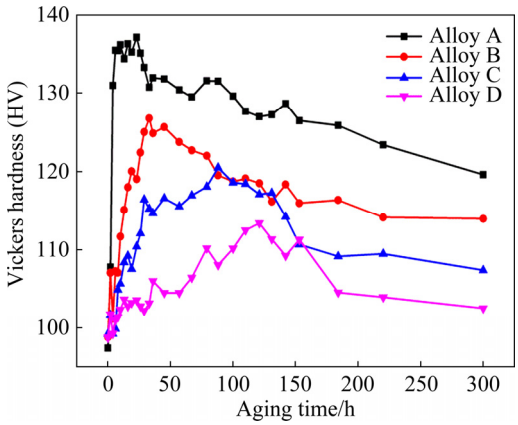

Fig. 10 Age-hardening curves of as-rolled Mg−Gd−Zn(−Al) alloys aged at 220 °C

B is obtained after 33 h, and its value is HV 126.72. Alloy C obtains a peak hardness of HV 120.48 after 88 h. However, the as-rolled Alloy D exhibits relatively poor age hardening behavior, and the peak hardness is obtained after 121 h, with a value of HV 113.39. With the increase of Al content, the age hardening response of the as-rolled alloys decreases gradually. The formation of LPSO and Al−Gd phases results in a decrease of Gd content in the α-Mg matrix, which results in a considerably low and slow age hardening response of the Mg−Gd−Zn−Al alloys.

Figure 11 shows the bright-field TEM images of peak-aged Alloys A and B and the corresponding

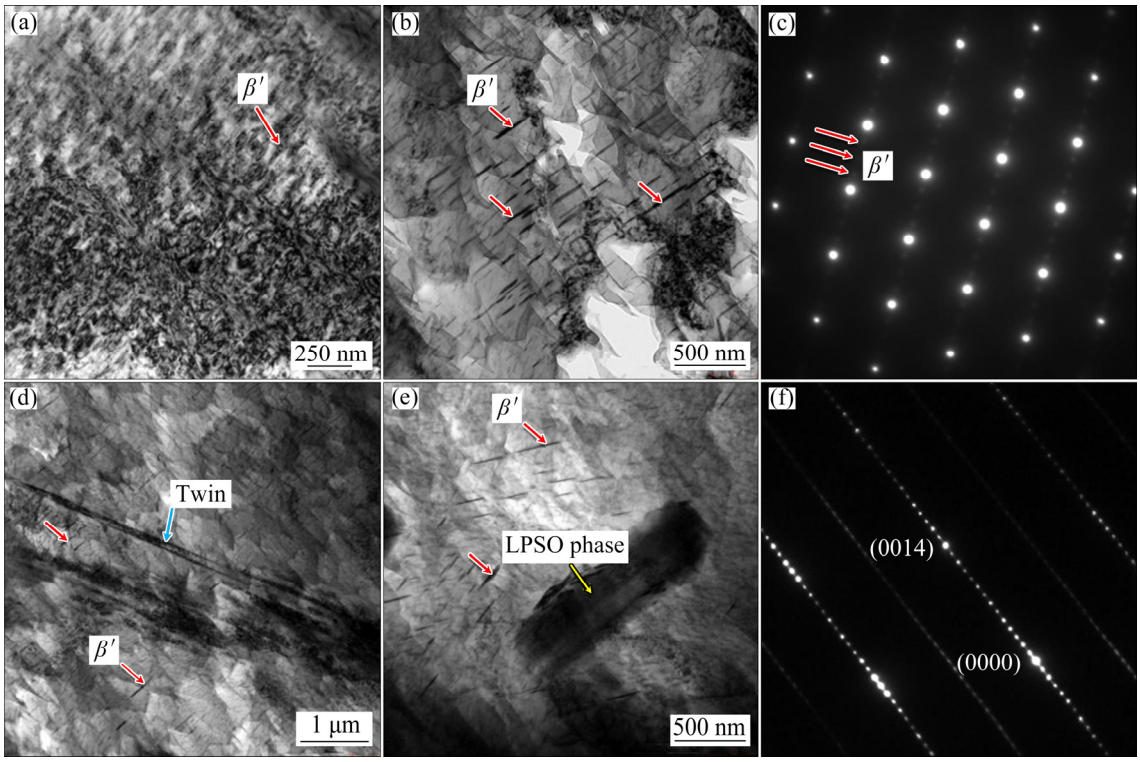

Fig. 11 Bright-field TEM images and corresponding SAED patterns of peak-aged Alloys A (a) and B (b−f) ((c) ***B***//$[0001]_{\alpha}$; (f) ***B***//$[11\bar{2}0]_{\alpha}$)

SAED pattern. A large number of elliptical precipitates (marked by red arrows) are observed in the matrix of peak-aged Alloys A and B. The SAED pattern shows that the three weaker diffraction spots are located at $1/4(01\bar{1}0)_{\alpha}$, $1/2(01\bar{1}0)_{\alpha}$ and $3/4(01\bar{1}0)_{\alpha}$. Such diffraction characteristics indicate that these ellipsoidal precipitates are β' phases with a bco structure. These precipitates exhibit a semi-coherent structure with α-Mg, which can effectively suppress the slipping of the basal planes. Compared with Al-free alloy, the peak-aged Alloy B exhibits sparse and fine precipitates. Figure 11(d) shows an extensive twin (marked by green arrow) surrounded by β' phases. This phenomenon is also consistent with Figs. 7(d) and 9(a). Some studies have shown that twin boundaries can effectively inhibit dislocation slip and improve the yield strength in a way similar to the grain boundary [35,36]. A bright-field TEM image of LPSO phase (marked by yellow arrow) accompanied by β' precipitates in the peak-aged Alloy C is shown in Fig. 11(e). The SAED pattern reveals that the LPSO phase is 14H-LPSO phase. Previous studies have suggested that there is a competitive demand for RE elements between 14H-LPSO phases and β' precipitates [28], which results in a higher density of β' precipitates in Al-free alloy than that in Al-containing alloys. This explains why the peak-aged Al-free alloy has a better age hardening response than the Al-containing alloys. ZHENG and CHEN [37] reported that an intercalation structure can be formed between the β' precipitates and the LPSO phases, which will hinder the coarsening of β' precipitates and LPSO phases. Both the appropriate volume fractions of the 14H-LPSO phases and the fine elliptical β' phases endow the peaked-aged alloy with good mechanical properties.

3.4 Mechanical properties

The tensile mechanical properties of the Mg−Gd−Zn(−Al) alloys under different conditions at ambient temperature are shown in Fig. 12. As-cast Alloy B exhibits the optimal mechanical properties, and the values of UTS, YTS and elongation are 219 MPa, 138 MPa and 3.7%, respectively, which may be attributed to the formation of 18R-LPSO phases with high elastic modulus and hardness [38]. However, as-cast Alloys C and D have relatively poor mechanical properties due to the presence of Al−Gd phases;

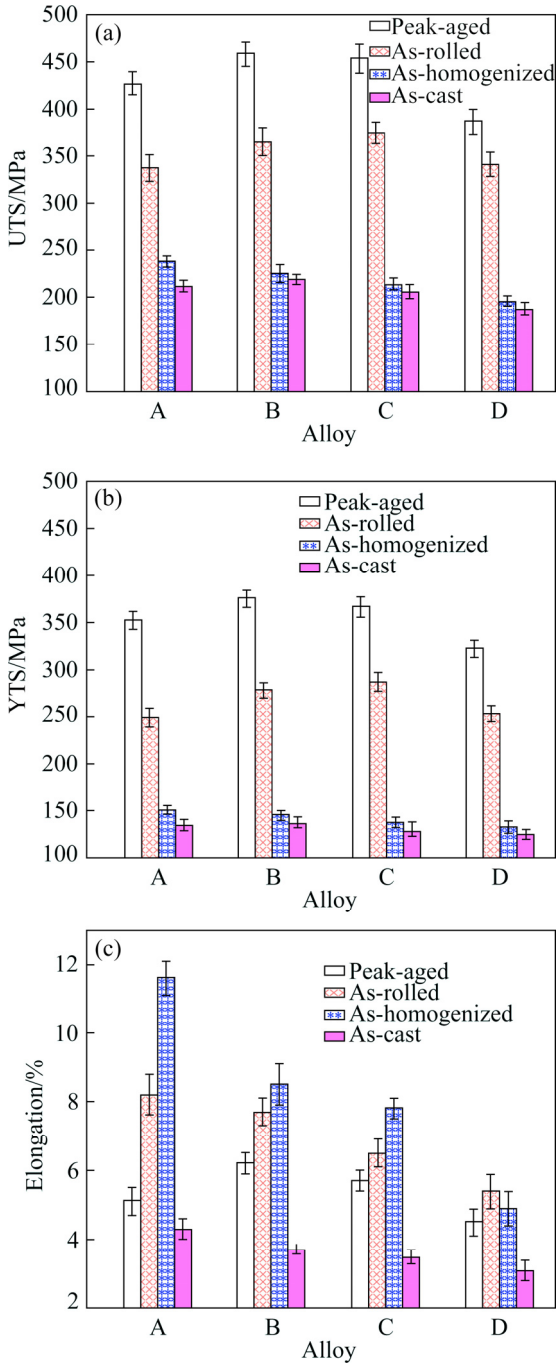

Fig. 12 Tensile properties of Mg−Gd−Zn(−Al) alloys in as-cast, as-homogenized, as-rolled and peak-aged conditions

especially for as-cast Alloy D with large Al_2Gd phases, the values of UTS, YTS and elongation are only 188 MPa, 125 MPa and 3.1%, respectively. After homogenization treatment, the mechanical properties of the Mg−Gd−Zn(−Al) alloys are improved due to the solution strengthening of the Gd elements and the second phase strengthening of 14H-LPSO phases. It is noted that the as-homogenized Al-free alloy exhibits the optimal mechanical properties, and the values of UTS and YTS are 238 MPa and 151 MPa, respectively, with the highest elongation of 11.6%. The tensile mechanical properties of the Mg−Gd−Zn(−Al) alloys decrease gradually with the increase of Al content. It is generally believed that the hard brittle phase with finer shape can improve the strength, but the severely coarsened phases (such as large bulk LPSO and Al_2Gd phases) are more sensitive to stress concentration [39]. The lamellar 14H-LPSO phases in Al-free alloy have a smaller average size than the bulk 14H-LPSO phases in Al-containing alloys, which can improve the mechanical properties more effectively [40].

After rolling, the tensile strength of the Mg−Gd−Zn(−Al) alloys is improved remarkably, which is mainly attributed to the grain refinement and fiber-like reinforcement of LPSO phase. For the as-rolled Al-free alloy, the values of UTS, YTS and elongation are 337 MPa, 249 MPa and 8.2%, respectively. The as-rolled Alloy C exhibits the optimal tensile strength, and the values of UTS and YTS are 374 MPa and 287 MPa, respectively. It is noteworthy that the elongation of the alloys with low Al content decreases significantly after rolling, especially Al-free alloy. This is due to the formation of sub-grains and excessive dislocation accumulation, resulting in stress concentration and ductility weakening of the as-rolled alloys [41]. Compared with Al-free alloy, Al-containing alloys have higher strength but lower plasticity. The higher strength is due to the finer grains and more LPSO phases in Al-containing alloys, while the weaker toughness is due to the existence of Al−Gd phases.

The mechanical properties of Mg−Gd−Zn(−Al) alloys are greatly improved after peak aging treatment except for the elongation. The UTS and YTS of the peak-aged Al-free alloy are improved significantly, with values of 427 MPa and 352 MPa, respectively. The peak-aged Alloy B exhibits the optimal mechanical properties and the UTS, YTS and elongation are 458 MPa, 375 MPa and 6.2%, respectively. However, Alloy D with large-sized Al_2Gd phase has small age hardening response, and the values of the UTS, YTS and elongation are 386 MPa, 322 MPa and 4.5%, respectively. Precipitation strengthening is the most dominant strengthening mechanism in the aging process. A large number of fine ellipsoidal β' phases

precipitating in the peak-aged alloys exhibit a semi-coherent structure with α-Mg, which can effectively inhibit the slipping of the basal planes and improve the tensile strength [42,43].

4 Conclusions

(1) The microstructures of the as-cast Al-free alloy consist of α-Mg and $(Mg,Zn)_3Gd$ phases. The addition of 0.4 wt.% of Al to the Mg−Gd−Zn alloy promotes the formation of 18R-LPSO phase ($Mg_{12}Gd(Al,Zn)$). With the increase of Al content to 0.7 wt.%, the 18R-LPSO phase disappears and a large number of $Al_{11}Gd_3$ and Al_2Gd phases distribute in the grains. Accompanied by the decrease of $(Mg,Zn)_3Gd$ phase, the content of $Al_{11}Gd_3$ and Al_2Gd increases with the increase of Al content.

(2) After homogenization treatment, $(Mg,Zn)_3Gd$, 18R-LPSO and some $Al_{11}Gd_3$ phases are transformed into the high-temperature stable 14H-LPSO phases. The volume fraction of the 14H-LPSO phases increases with the increase of Al content from 0 to 0.7 wt.%. The polygonal Al_2Gd and some clustered $Al_{11}Gd_3$ phases have good high-temperature stability.

(3) The 14H-LPSO and $Al_{11}Gd_3$ phases are pressed into the plate-shaped phases during hot rolling, while the Al_2Gd phases are not affected. All the as-rolled alloys exhibit a fine and uniform microstructure. The tensile strength of the alloys are improved remarkably due to the grain refinement and fiber-like reinforcement of LPSO phase.

(4) The age hardening response of the as-rolled alloys decreases gradually with the increase of Al content. The precipitation of the β' phases in the peak-aged alloys can effectively inhibit the slipping of the basal planes, resulting in precipitation hardening, and significantly improving the strength. The peak-aged Alloy B exhibits the optimal mechanical properties and the UTS, YTS and elongation are 458 MPa, 375 MPa and 6.2%, respectively.

Acknowledgments

The authors are grateful for the financial supports from the Natural Science Foundation of Hunan Province, China (No. 2018JJ2365), the Outstanding Youth Scientific Research Project of Hunan Education Department, China (No. 20B533), the Science and Technology Innovation Program of Hunan Province, China (No. 2020RC1011), the Graduate Scientific Research Innovation Project of Hunan Province, China (No. CX20211280), the Science and Technology Innovation Leading Plan of High Tech Industry in Hunan Province, China (No. 2020GK2033), and the Key Scientific Research Project of Hunan Provincial Department of Education, China (No. 20A455).

References

[1] SMOLA B, STULIKOVA I, PELCOVA J, MORDIKE B. Significance of stable and metastable phases in high temperature creep resistant magnesium-rare earth base alloys [J]. Journal of Alloys and Compounds, 2004, 378: 196−201.

[2] HOU Cai-hong, YE Zhi-song, QI Fu-gang, WANG Qing, LI Lian-hui, OUYANG Xiao-ping, ZHAO Nie. Effect of Al addition on microstructure and mechanical properties of Mg−Zn−Sn−Mn alloy [J]. Transactions of Nonferrous Metals Society of China, 2021, 31: 1951−1968.

[3] LU R P, WANG J F, CHEN Y L, QIN D Z, YANG W X, WU Z S. Effects of heat treatment on the morphology of long-period stacking ordered phase, the corresponding damping capacities and mechanical properties of Mg−Zn−Y alloys [J]. Journal of Alloys and Compounds, 2015, 639: 541−546.

[4] DING Zhi-bing, ZHAO Yu-hong, LU Ruo-peng, YUAN Mei-ni, WANG Zhi-jun, LI Hui-jun, HOU Hua. Effect of Zn addition on the microstructure and mechanical properties of cast Mg−Gd−Y−Zr alloys [J]. Transactions of Nonferrous Metals Society of China, 2019, 29: 722−734.

[5] HANTZSCHE K, BOHLEN J, WENDT J, KAINER K U, YI S B, LETZIG D. Effect of rare earth additions on microstructure and texture development of magnesium alloy sheets [J]. Scripta Materialia, 2010, 63: 725−730.

[6] CHINO Y, KADO M, MABUCHI M. Enhancement of tensile ductility and stretch formability of magnesium by addition of 0.2wt.%(0.035 at.%)Ce [J]. Materials Science and Engineering A, 2008, 494: 343−349.

[7] YAN H, CHEN R, ZHENG N, LUO J, KAMADO S, HAN E. Effects of trace Gd concentration on texture and mechanical properties ofhot-rolled Mg−2Zn−*x*Gd sheets [J]. Journal of Magnesium and Alloys, 2013, 1: 23−30.

[8] LI Q, WANG Q D, WANG Y X, ZENG X Q, DING W J. Effect of Nd and Y addition on microstructure and mechanical properties of as-cast Mg−Zn−Zr alloy [J]. Journal of Alloys and Compounds, 2007, 427: 115−123.

[9] YAMASAKI M, ANAN T, YOSHIMOTO S, KAWAMURA Y. Mechanical properties of warm-extruded Mg−Zn−Gd alloy with coherent 14H long periodic stacking ordered structure precipitate [J]. Scripta Materialia, 2005, 53: 799−803.

[10] GAO X, NIE J F. Enhanced precipitation-hardening in Mg−Gd alloys containing Ag and Zn [J]. Scripta Materialia, 2008, 58: 619−622.

[11] YOKOBAYASHI H, KISHIDA K, INUI H, YAMASAKI M, KAWAMURA Y. Enrichment of Gd and Al atoms in the quadruple close packed planes and their in-plane long-range ordering in the long period stacking-ordered phase in the Mg−Al−Gd system [J]. Acta Materialia, 2011, 59: 7287−7299.

[12] KISHIDA K, INOUE A, YOKOBAYASHI H, INUI H. Deformation twinning in a Mg−Al−Gd ternary alloy containing precipitates with a long-period stacking-ordered (LPSO) structure [J]. Scripta Materialia, 2014, 89: 25−28.

[13] KISHIDA K, YOKOBAYASHI H, INUI H, YAMASAKI M, KAWAMURA Y. The crystal structure of the LPSO phase of the 14H-type in the Mg−Al−Gd alloy system [J]. Intermetallics, 2012, 31: 55−64.

[14] CAO P, QIAN M, STJOHN D H. Effect of manganese on grain refinement of Mg−Al based alloys [J]. Scripta Materialia, 2006, 54: 1853−1858.

[15] CAO P, STJOHN D H, QIAN M. The effect of manganese on the grain size of commercial AZ31 alloy [J]. Materials Science Forum, 2005, 488−489: 139−142.

[16] QIU D, ZHANG M X, TAYLOR J A, KELLY P M. A new approach to designing a grain refiner for Mg casting alloys and its use in Mg−Y-based alloys [J]. Acta Materialia, 2009, 57: 3052−3059.

[17] QIU D, ZHANG M X, KELLY P M. Crystallography of heterogeneous nucleation of Mg grains on Al_2Y nucleation particles in an Mg−10wt.%Y alloy [J]. Scripta Materialia, 2009, 61: 312−315.

[18] DAI J C, ZHU S M, EASTON M, ZHANG M X, QIU D, WU G H, LIU W C, DING W J. Heat treatment, microstructure and mechanical properties of a Mg−Gd−Y alloy grain-refined by Al additions [J]. Materials Science and Engineering A, 2013, 576: 298−305.

[19] ZHAO Z D, CHEN Q, WANG Y B, SHU D Y. Microstructures and mechanical properties of AZ91D alloys with Y addition [J]. Materials Science and Engineering A, 2009, 515: 152−161.

[20] FANG C F, LIU G X, HAO H, WEN Z H, ZHANG X G. Effect of Al addition on microstructure, texture and mechanical properties of Mg−5Gd−2.5Y−2Zn alloy [J]. Journal of Alloys and Compounds, 2016, 686: 347−355.

[21] DING Z, LU R, ZHAO Y, HOU H, CHENG P, BU Z, ZHANG P. The microstructure and mechanical properties of as-cast Mg−10Gd−3Y−*x*Zn−0.6Zr (*x*=0, 0.5, 1 and 2 wt.%) Alloys [J]. Materials Research-Ibero-american Journal of Materials, 2018, 21: e20170992.

[22] BIAN L P, WANG L P, ZHOU Y Y, ZENG H H, ZHAO Y L, LIANG W. Effects of different amounts of $AlCa_2$ addition on the microstructure and mechanical properties of Mg−Gd−Zn alloy [J]. Materials Science and Engineering A, 2017, 698: 12−17.

[23] FANG C F, LIU G X, LIU X T, HAO H, ZHANG X G. Significant texture weakening of Mg−8Gd−5Y−2Zn alloy by Al addition [J]. Materials Science and Engineering A, 2017, 701: 314−318.

[24] HONMA T, OHKUBO T, KAMADO S, HONO K. Effect of Zn additions on the age hardening of Mg−2.0Gd−1.2Y−0.2Zr alloys [J]. Acta Materialia, 2007, 55: 4137−4150.

[25] WANG J F, WANG K, HOU F, LIU S J, PENG X, WANG J X, PAN F S. Enhanced strength and ductility of Mg−RE−Zn alloy simultaneously by trace Ag addition [J]. Materials Science and Engineering A, 2018, 728: 10−19.

[26] DAI J C, EASTON M, ZHU S M, WU G H, DING W J. Grain refinement of Mg−10Gd alloy by Al additions [J]. Journal of Materials Research, 2012, 27: 2790−2797.

[27] HUANG S, WANG J F, HOU F, HUANG X H, PAN F S. Effect of Gd and Y contents on the microstructural evolution of long period stacking ordered phase and the corresponding mechanical properties in Mg−Gd−Y−Zn−Mn alloys [J]. Materials Science and Engineering A, 2014, 612: 363−370.

[28] DING Z, ZHAO Y, LU R, PEI H, HOU H. Microstructure evolution and mechanical properties of Mg−10Gd−3Y−*x*Zn−0.6Zr alloys [J]. Journal of Materials Research, 2018, 33: 1797−1805.

[29] CHENG P, ZHAO Y H, LU R P, HOU H. Effect of the morphology of long-period stacking ordered phase on mechanical properties and corrosion behavior of cast Mg−Zn−Y−Ti alloy [J]. Journal of Alloys and Compounds, 2018, 764: 226−238.

[30] BOHLEN J, NURNBERG M R, SENN J W, LETZIG D, AGNEW S R. The texture and anisotropy of magnesium−zinc−rare earth alloy sheets [J]. Acta Materialia, 2007, 55: 2101−2112.

[31] HIRSCH J, AL-SAMMAN T. Superior light metals by texture engineering: Optimized aluminum and magnesium alloys for automotive applications [J]. Acta Materialia, 2013, 61: 818−843.

[32] PARK S H, YU H, BAE J H, YIM C D, YOU B S. Microstructural evolution of indirect-extruded ZK60 alloy by adding Ce [J]. Journal of Alloys and Compounds, 2012, 545: 139−143.

[33] WEN Q, DENG K, SHI J, ZHANG B, LIANG W. Effect of Ca addition on the microstructure and tensile properties of Mg−4.0Zn−2.0Gd alloys [J]. Materials Science and Engineering A, 2014, 609: 1−6.

[34] XU C, ZHENG M Y, XU S W, WU K, WANG E D, KAMADO S, WANG G J, LV X Y. Ultra high-strength Mg−Gd−Y−Zn−Zr alloy sheets processed by large-strain hot rolling and ageing [J]. Materials Science and Engineering A, 2012, 547: 93−98.

[35] LU L, CHEN X, HUANG X, LU K. Revealing the maximum strength in nanotwinned copper [J]. Science, 2009, 323: 607−610.

[36] SHEN Y F, LU L, LU Q H, JIN Z H, LU K. Tensile properties of copper with nano-scale twins [J]. Scripta Materialia, 2005, 52: 989−994.

[37] ZHENG J, CHEN B. Interactions between long-period stacking ordered phase and β' precipitate in Mg−Gd−Y−Zn−Zr alloy: Atomic-scale insights from HAADF-STEM [J]. Materials Letters, 2016, 176: 223−227.

[38] SHAO X H, YANG Z Q, MA X L. Strengthening and toughening mechanisms in Mg−Zn−Y alloy with a long period stacking ordered structure [J]. Acta Materialia, 2010, 58: 4760−4771.

[39] XU D K, TANG W N, LIU L, XU Y B, HAN E H. Effect of W-phase on the mechanical properties of as-cast Mg−Zn−Y−Zr alloys [J]. Journal of Alloys and Compounds, 2008, 461: 248−252.

[40] WANG J F, SONG P F, HUANG S, PAN F S. High-strength and good-ductility Mg−RE−Zn−Mn magnesium alloy with long-period stacking ordered phase [J]. Materials Letters, 2013, 93: 415−418.

[41] XU C, ZHENG M Y, XU S W, WU K, WANG E D, KAMADO S, WANG G J, LV X Y. Microstructure and mechanical properties of rolled sheets of Mg−Gd−Y−Zn−Zr alloy: As-cast versus as-homogenized [J]. Journal of Alloys and Compounds, 2012, 528: 40−44.

[42] JIA Lin-yue, DU Wen-bo, WANG Zhao-hui, LIU Ke, LI Shu-bo, YU Zi-jian. Dual phases strengthening behavior of Mg−10Gd−1Er−1Zn−0.6Zr alloy [J]. Transactions of Nonferrous Metals Society of China, 2020, 30: 635−646.

[43] HAN X Z, XU W C, SHAN D B. Effect of precipitates on microstructures and properties of forged Mg−10Gd−2Y−0.5Zn−0.3Zr alloy during ageing process [J]. Journal of Alloys and Compounds, 2011, 509: 8625−8631.

Al 添加对 Mg−Gd−Zn 合金显微组织和力学性能的影响

丁志兵[1,2]，张 帅[1,2]，赵宇宏[3]，陈东瑞[1,2]，邹利华[1,2]，陈志刚[1,2]，郭文敏[1,2]，苏再军[1,2]，侯 华[3]

1. 邵阳学院 机械与能源工程学院，邵阳 422000；
2. 邵阳学院 高效动力系统智能制造湖南省重点实验室，邵阳 422000；
3. 中北大学 材料科学与工程学院，太原 030051

摘 要：研究不同 Al 含量(0, 0.4%, 0.7%和 1.0%，质量分数)Mg−15.3Gd−1Zn 合金的显微组织演变和力学性能。显微组织分析表明，添加 0.4%Al 有利于 Mg−Gd−Zn 合金中 18R-LPSO 相($Mg_{12}Gd(Al,Zn)$)的形成。随着 Al 含量的增加，$Al_{11}Gd_3$ 和 Al_2Gd 相含量增加，同时$(Mg,Zn)_3Gd$ 相含量减少。均匀化处理后，$(Mg,Zn)_3Gd$、18R-LPSO 和部分 $Al_{11}Gd_3$ 相转变为高温稳定的 14H-LPSO 相。颗粒状 Al−Gd 相可通过粒子激发形核(PSN)机制促进动态再结晶的形核。由于晶粒的细化和纤维状长程堆垛有序(LPSO)相的强化，轧制态合金的抗拉强度得到显著提高。峰时效态合金中的 β'析出相能显著提高合金的强度。峰时效态下含 0.4%Al 的合金具有优异的力学性能，该合金的抗拉强度、屈服强度和伸长率分别为 458 MPa、375 MPa 和 6.2%。

关键词：Mg−Gd−Zn−Al 合金；长程堆垛有序相；β'相；力学性能

(Edited by Bing YANG)